Temperatures of the pyroclastic density currents deposits emplaced in the last 22 kyr at Somma-Vesuvius (Italy)

(Article begins on next page)

18 April 2024

Temperatures of the pyroclastic density currents deposits emplaced in the last 22 kyr at Somma-Vesuvius (Italy)

Elena Zanella[1,2,*], Roberto Sulpizio[3, 4], Lucia Gurioli[5], Roberto Lanza[1,2]

1 – Dipartimento di Scienze della Terra, Università di Torino, Italy

2 – ALP – Alpine Laboratory of Paleomagnetism, Peveragno, Italy

3 – Dipartimento di Scienze della Terra e Geoambientali, via Orabona 4, 70125, Bari, Italy

4 – IDPA-CNR, via M. Bianco 9, Milan, Italy

5 - OPGC, Laboratoire Magmas et Volcans, Clermont-Ferrand, France

*Corresponding author (e-mail: elena.zanella@unito.it)

Number of words of text: 6611

Number of references: 59

Number of tables: 3

Number of figures: 6

Abbreviated title: Deposit temperature of Somma-Vesuvius PDCs

Abstract

The temperature of the deposits (T_{dep}) emplaced by the pyroclastic density current (PDC) generated by the seven major explosive eruptions from Somma-Vesuvius during the last 22 kyr were investigated using the thermal remanent magnetization of lithic clasts embedded within the deposits. New data are presented for the Pomici di Base, Greenish Pumice, Mercato and 1631 AD deposits and compared to the literature data from the Avellino, 79 AD-Pompeii and 472 AD-Pollena eruptions. The T_{dep} mainly fall in the range 270-370 °C, and no significant correlation is evidenced between sedimentological features, eruptive and depositional processes and the final T_{dep}. The admixture of ambient air during the runout appears the most effective process to cool the temperature of the ash and gases of the PDC, and is thus the main factor affecting the deposit temperature.

Somma–Vesuvius is one of the most hazardous volcanoes in the world, with more than 650,000 people living within 10 km of the summit crater. During the last 22 kyr of activity, several explosive eruptions of large magnitude and intensity have occurred (Santacroce 1987; Cioni *et al.* 2008; Santacroce *et al.* 2008), which generated large-volume pyroclastic density currents (PDCs, Gurioli *et al.* 2010). PDCs are hot, gravity-driven currents of volcanic particles and gas that travel at velocities of tens to hundreds of meters per second (Druitt 1998; Branney & Kokelaar 2002; Sulpizio & Dellino 2008), often causing near-complete destruction of widespread areas (Tilling & Lipman 1993). The hazards they pose are related to their temperature, particle concentration, ballistic content, dynamic pressure, and ability to inundate and bury the environment under thick deposits (Baxter *et al.* 1998, 2008; Esposti Ongaro *et al.* 2002). Because of their devastating impact, PDCs deposits at Somma-Vesuvius have been studied using many techniques, including studies of their dispersal, thickness, volume and extent (Gurioli *et al* 2002; Sulpizio *et al.* 2007; 2010; Gurioli *et al* 2010), modeling of their processes and hazards (Rossano *et al.* 1998; Dobran *et al* 1994, Esposti Ongaro *et al* 2008), and their impact on people and buildings (Baxter *et al* 2008; Gurioli *et al.* 2005; Zuccaro *et al.* 2008; Di Vito *et al.* 2009). For some eruptions, physical parameters of PDCs, such as velocity, concentration of particles, thickness (Sulpizio *et al.* 2007; 2010; Mele *et al.* 2011), palaeo flow directions (Gurioli *et al.* 2002; 2005; 2007; Di Vito *et al.* 2009), and temperature of the deposits (Cioni *et al.* 2004; Zanella *et al.* 2007; 2008; Di Vito et al. 2009) have been estimated. In this paper, we review previous studies and present new data about the deposit temperature (T_{dep}) of the PDCs emplaced during the whole eruptive history of Somma-Vesuvius. The aim is to provide a comprehensive framework of deposit temperature of PDCs at Somma-Vesuvius, derived from thermal remanent magnetization (TRM) measurements on lithic clasts embedded in PDC deposits. The T_{dep} (here defined as the equilibrium temperature acquired after deposition; Cioni et al. 2004) data will be critically discussed in the light of the whole range of eruptive parameters (temperature and chemistry of the magma and intensity of the eruption), eruptive (magmatic versus phreatomagmatic) and depositional processes (facies of PDC deposits), in order to define the common general processes that control the final T_{dep} of the deposits. This work represents the first comprehensive attempt at assessment of PDC emplacement temperature at Somma-Vesuvius, and provides important data useful for the improvement of knowledge on PDC dynamics and for a better evaluation of associated hazard.

Main characteristics of the PDC deposits

The Somma–Vesuvius volcanic complex consists of an older stratovolcano (Mt Somma) cut by a multistage summit caldera, within which the recent Vesuvius cone has grown. In the last 22 kyr,

four main Plinian "caldera-forming" eruptions have occurred (Pomici di Base, Mercato, Avellino, and Pompeii; Fig. 1, Table 1), as well as three major sub-Plinian I eruptions (Greenish, 472 AD-Pollena, and 1631 AD; sub-Plinian I category of Cioni *et al.* 2008) and several other significant events (sub-Plinian II, violent strombolian, continuous ash emission, and mildly strombolian categories of Cioni *et al.* 2008). Only the Plinian and sub-Plinian I events produced widespread PDC deposits (Rosi & Santacroce 1983; Cioni *et al.* 2003; Sulpizio *et al.* 2005; Rosi *et al.* 1993; Gurioli *et al.* 2010; Mele *et al* 2011, Sulpizio *et al.* 2010). Following Gurioli *et al.* (2010), the main characteristics of these deposits can be described in terms of their dispersion, sedimentology, thickness, grain size and componentry (Table 1):

- five out of seven eruptions dispersed PDCs radially, covering the whole volcano and the surrounding plain. These distributions, depending on the position of the palaovent and the caldera wall, are more or less symmetric (Pomici di Base, Mercato and Pollena) or strongly assymetric (Avellino and Pompeii). In contrast, the PDC deposits from the Greenish Pumice eruption mainly occur on the northern slopes of Mt Somma, and the PDC deposits from the 1631 AD eruption, form several lobes in the southern and western sectors of the volcano.

- PDC deposits are distributed over all flanks of the volcano, generally showing significant thickening in the main valleys, mantling the interfluves between the valleys and forming prograding depositional fans at the end of the main valleys:

- The present caldera wall acted as a barrier only for the 1631 AD PDCs; in all the other eruptions, PDCs overtopped this wall and inundated the northern sector. However, in cases where the vent was located far from the caldera wall, the presence of the wall influenced the deposition in the northern sector (e.g. Avellino euption). For the Greenish eruption, whose PDC deposits are confined in the northern sector, the still standing East-South caldera wall probably stopped these PDCs for propagating toward these sectors.

- Most of the PDC deposits were dispersed within 8-10 km from the inferred vent. Only two PDC deposits, generated during the Avellino and Pompeii eruptions, extend more than 20 km from the vent.

- The volume of the PDC deposits generated during each eruption ranges between 0.02 and 1 km^3 and their maximum cumulative thickness ranges between 8-35 meters.

- The lithic components make up 10-50% of the magmatic and 40 to 65% of the phreatomagmatic deposits and the median grain size ranges between -3 and 2 ϕ. Apart from local fines-poor facies, the deposits are generally composed for more than 50% in volume of a matrix of coarse and fine ash.

Methods

Aramaki & Akimoto (1957) first showed the potential use of rock magnetism to estimate the emplacement temperature of pyroclastic deposits. With a few exceptions (Chadwick 1971; Hoblitt & Kellogg 1979; Kent *et al.* 1981), their paper received little attention and only in the last twenty-five years have palaeomagnetists and volcanologists revived their suggestion and improved sampling and analytical procedures. A basic account of the method is provided by Paterson et al. (2010) together with a list of the papers on the subject published at that date.

Classicaly, the model for estimating the emplacement temperature of a pyroclastic deposit assumes that cold lithic clasts were incorporated and heated into a hot mixture of ash and gases travelling across the palaeotopographical surface, and were eventually embedded within the fine-grained matrix of the deposit. They then completed their thermal equilibration within the PDC deposit, and after cool down together with the whole deposit. The process of re-heating and cooling back to the ambient temperature results in a magnetic overprint. The method relies on two basic properties of volcanic rocks:

1) the ferromagnetic grains in a rock acquire a stable thermal remanent magnetization (TRM) at different temperature values, depending up on mineralogy, size and shape of each grain. Below the blocking temperature (T_b) of a grain, its remanence may be regarded as stable. The ferromagnetic grains in a rock usually show large variations in shape and size, which strongly affect the blocking temperature. The TRM is therefore acquired throughout a wide spectrum of T_b;

2) the TRMs of grains with different T_b are mutually independent and they add to each other to give the total TRM of the rock. In other words, as the rock cools down, the remanences acquired in different parts of the T_b spectrum add up, and the process is reversible: if the rock is re-heated, each portion of the remanence is lost in the same part of the T_b spectrum it was acquired. As a consequence, cold lithic fragments re-heated by a hot pyroclastic cloud lose a part of their primary TRM, acquired when the parent rock formed, and acquire a secondary TRM component when cooling within the pyroclastic deposit.

The magnetic overprint depends on the relation between the T_b spectrum of each individual lithic clast and the re-heating temperature T_r, which can be investigated by stepwise thermal demagnetization. Cioni *et al.* (2004) distinguished four basic types (Fig. 2):

1) type A clasts have a single TRM component whose direction is casually scattered from clast to clast and different from the palaeomagnetic direction at the time of the eruption, which is recorded by the fine-grained matrix. In this case, T_r was lower than the lowest T_b value, no remanence was unblocked and the clast did not record the re-heating. The TRM is the primary one, but the primary geographic direction got lost when the clasts broke off from the original outcrop;

5

2) type B clasts have a single TRM component whose direction is similar in all clasts and close to the direction recorded by the fine-grained matrix. In this case, T_r was higher than the highest T_b value and all primary remanence was unblocked. The clasts acquired a secondary TRM parallel to the ambient field during cooling;

3) type C clasts have two TRM components with different directions and T_b spectra. The direction of the high-T_b component is casual, that of the low-T_b component is close to the palaeomagnetic direction of the fine-grained matrix. The threshold between the two spectra gives the T_r value. The grains with high T_b were unaffected by re-heating and kept their primary TRM, those with low-T_b lost the primary remanence and acquired a new secondary TRM;

4) type D clasts have two TRM components with partially overlapping T_b spectra. They are similar to type C, but the two components are not clearly separated and the T_r value can only be defined within the overlap interval. In the case in which magnetite is the primary ferromagnetic mineral, this behaviour may be explained by the occurrence of large, multi-domain grains or of a chemical remanent magnetization (CRM) due to the syneruptive oxidation of magnetite to maghemite (McClelland 1996; Bardot & McClelland 2000; Paterson *et al.* 2010).

The above model is oversimplified because it disregards the thermal history of the lithic clasts and does not take their size into account. Besides the cold clasts picked up along the volcano slope downstream from the vent, the deposit may also include juvenile fragments and those eroded from the conduit wall, fragments whose initial temperature is as high as that of the ash and gas cloud. These hot fragments cool by radiation less than the cloud material because the run-out time is short and the temperature of the cloud strongly decreases by progressive admixing of air. Whereas the cold fragments are re-heated by the heat they absorb from the deposit, the hot ones convey heat to it. The T_r value given by thermal demagnetization is therefore higher than the T_{dep}. Archaeological remains embedded in the PDC deposits give the best T_r estimates because their thermal history is known: they were definitely cold before being embedded in the deposit. In the case of Pompeii and Herculaneum, the Roman cities buried by the 79 AD eruption, a good agreement was found between the temperature values derived from tiles and potsherds and those from lithic clasts (Gurioli *et al.* 2005; Zanella *et al.* 2007).

A second point is that the time needed to reach thermal equilibrium between a lithic fragment and the fine-grained material increases with size. The thermal diffusivity of common magmatic rocks is in the range of $10-6$ m^2/s (e.g. Vosteen & Schellschmidt 2003), although up to one order of magnitude variations are possible as a function of porosity, density and temperature of the lithic fragment (Velinov *et al.* 1993). This range of diffusivity is comparable to that of liquid water (James 1968), and at least two orders of magnitude less than that of dry air at 127–227 °C. This

6

means that lava fragments entrapped in the flow at ambient temperature significantly increase their temperature in a time that is usually longer than flow duration, at least for fragments coarser than 2 cm (Cioni *et al.* 2004). This implies that the most significant amount of heat flow going from hot material to the cooler fragments occurs within the deposit (Sulpizio *et al.* 2008), and that $T_r \approx T_{dep}$ is true only for lithic fragments finer than 2 cm. In lithic lag breccias, where cold lithic fragments might make-up >50% of the total deposit, the cold sink effect means that the temperature of emplacement would be drastically under-estimated.

While they are re-heated, the whole deposit cools down and equilibrium is reached at a temperature value lower than T_{dep} and thus $T_r < T_{dep}$, as typical for clasts embedded within the upper portion of thin deposits or when entrainment of water occurs during emplacement. Downey & Tarling (1984) investigated the TRM variation from the surface to the inside of blocks 10-15 cm in size and showed that the re-heating affected only the outer portions, to a depth of a couple of cm.

In conclusion, the dispersion of the experimental T_r values is expected to be small for cold lapilli-size lithic clasts embedded in the central part of a thick pyroclastic deposit. The less the characteristics of the deposit comply with the model, the more dispersion increases. Taking into account that the thermal history of the individual clasts is unknown, we consider that the best approach to evaluate T_{dep} is to look for the mutual consistency of the experimental T_r values at the sampling site scale. The analysis of diagrams such as those in Fig. 2 yields the T_r range of each individual clast and the overlap of the ranges gives a reasonable estimate of T_{dep}.

Investigation of the deposition temperature of pyroclastic deposits has long been confined to proximal facies, the only ones that include clasts large enough to be cut to standard palaeomagnetic specimens, cubes or cylinders 8 to 11 cm^3 in volume. Application to distal facies requires a technique to measure small, irregularly shaped clasts while maintaining consistent orientation with respect to the magnetometer sensor after each step of thermal demagnetization. Cioni *et al.* (2004) put the clasts in cubic plastic boxes filled with white moulding paste: after each measurement, the specimen is removed, heated in the furnace and then put back in the mould, ready to be measured at the next step. Due to the high intensity of remanence in volcanic rocks, even small clasts a few millimeters in size can be accurately measured.

Finally, Bardot & McClelland (2000) remarked that a portion of the TRM of a clast exposed to a magnetic field relaxes and gives rise to a viscous remanent magnetization (VRM) parallel to the field. In the case of recent deposits, both the TRM overprint and the VRM are aligned close with the present-day field. During thermal demagnetization, therefore, the maximum value of the unblocking temperature needed to remove the VRM, if any, corresponds to the lowest limit of the T_r value that can be resolved. This limit increases with the age of the deposit, because the VRM unblocking

temperature depends on the exposure time. In our case, the time-temperature approximate relation proposed by Bardot & McClelland (2000) set the limit from 115 °C to 140 °C for the 1631 AD and the 22 ka Pomici di Base deposits, respectively, the youngest and oldest deposits in this study.

Sampling and measurements

The deposits of the eruption of Avellino, Pompeii and Pollena PDCs have been extensively sampled and studied by present authors in previous papers (Cioni *et al.* 2004; Zanella *et al.* 2007; Zanella *et al.* 2008; Di Vito *et al.* 2009) and the results are summarized in Table 1. For the present study, we sampled the deposits of the other eruptions that produced extensive PDC deposits at Somma-Vesuvius, whose T_{dep} has not yet been investigated in the literature:

1) Pomici di Base - 22 ka (Bertagnini *et al.* 1998; Santacroce *et al.* 2008);
2) Greenish - 19 ka (Cioni *et al.* 2003);
3) Mercato - 8.5 ka (Mele *et al.* 2011; Zanchetta *et al.* 2011)
4) 1631 AD (Rosi *et al.* 1993).

The number of sampling sites for these eruptions is reduced with respect to those previously studied because of the limited exposure of deposits and the paucity of lithic clasts suitable for TRM measurement.

A total of 136 samples less than 2-3 cm in size were collected from 11 sites and were measured at the ALP Laboratory (Peveragno – Italy), using AGICO spinner magnetometers JR-5 and JR-6. Thermal demagnetization was run at 10-12 steps, using Schonstedt and ASC commercial furnaces. Whenever possible, each clast was cut into two pieces and the twin specimens demagnetized at 40 °C steps, one starting at 100 °C, the other at 120 °C. Magnetic susceptibility was measured after each step to check for mineralogical alteration, if any, due to heating. Comparison of the two runs results in narrowing the T_r range of the clast. The analysis of the intensity decay curves, Zijderveld (1967) diagrams and equal-area projections yields the type distribution of the clasts (Table 1): roughly half of the samples are type C, half type D; only two type B clasts occur in the 1631 deposits. Representative examples are shown in the previous section (Fig. 2), whereas Figure 3 shows some selected cases:

- the Zijderveld diagram of the sample PdB4A (Fig. 3a, b) shows that the NRM consists of three components and two temperature thresholds are apparent. The clast was first embedded within a deposit and heated to $T_{r1} = 380\text{-}420$ °C. The pyroclastic deposit was eventually eroded and the clast

picked up by a PDC of the Pomici di Base eruption and heated to $T_{r2} = 260$-300 °C. The young re-heating temperature was lower than the old, $T_{r2} < T_{r1}$, which therefore is still recorded by the clast.

- in sample Br3A (Fig. 3c, d) from the same eruption, the intensity of the low-T_b component is very low. The threshold between the low- and the high-T_b components may be unclear and the T_r range may only be defined in a wide interval.

Figure 4 shows the location of the sampling sites in a digital elevation model of Vesuvius. The insets report the T_r range of all the clasts collected at each site. The T_r range corresponds to the demagnetization step of 40° C for most type C clasts and is on the order of 80 to 120 °C for type D clasts. In a few cases, only the lower limit of the T_r range may be defined, as in the case of specimen Mc9-2-5 in the PDC8 of Mercato (Fig. 4). Within each individual insets, the whole of the T_r ranges, with the exception of few outliers, defines an overlap interval that yields the estimate of the deposition temperature (T_{dep}) at the site. At the two sites corresponding to PDC5 and PDC8 of the Mercato deposits, the definition of the overlap is low.

The T_{dep} values are on the order of 340-360 °C for the deposits of the Pomici di Base and Greenish eruptions, and 380-400 °C for the AD 1631 deposits. The deposits of PDC3 and PDC8 of the Mercato eruption are on the order of 360-400 °C, whereas those of other PDCs are as a high as 380-420 °C.

Collection of small clasts makes it possible to investigate the deposition temperature at distal sites, yet it confronts two main problems:

1) the field orientation of small clasts is seldom accurate and can be impossible to measure, so that most directions of the TRM components are only given in the specimen reference system. This disadvantage is negligible in the evaluation of T_r, which is done on the ground of the difference between the directions and not on their absolute values, but affects the definition of the low-T_b component, whose direction should be close to the palaeomagnetic direction at the time of eruption.

Figure 5 shows the directions of the secondary TRM component derived from clasts of the 1631 AD deposits. Five type C clasts yield a ChRM direction, whereas six type D clasts yield a great remagnetization circle (Halls 1978). The mean direction was therefore calculated according to McFadden & McElhinny (1998). Table 2 compares the mean direction of the clasts from the deposits of individual eruptions of Somma-Vesuvius with those of the primary TRM derived from the fine-grained matrix, i.e. the palaeomagnetic directions. It is clear from the values of the statistical parametres that the dispersion of the secondary directions from lithic clasts is higher than that of the primary directions from the fine-grained matrix. As for Pollena deposits studied by Paterson et al. (2010), the dispersion of the mean secondary directions is similar to or higher than that in Table 2. According to these authors, secondary directions close to the palaeomagnetic

direction are a good evidence for a low-T_b component of thermal origin acquired during the post-depositional cooling. The actual situation, however, is far complicated. In the case of the young rocks from Somma-Vesuvius, the high dispersion is usually below the quality standards required for archaeomagnetic dating. The mean secondary directions are statistically indistinguishable from the palaeosecular variation that occurred during the time lapses between the various eruptions as well as over longer time and give no definite evidence for their age. In conclusion, the agreement between the secondary and palaeomagnetic directions has little statistical value. It is a reasonable indication that both directions were acquired at the same time, but it is not definitive. Finally, it is worth remarking that secondary directions are essential to define the deposition temperature of clasts that carry a single magnetization component, as Aramaki & Akimoto (1957) first propounded. In this case, the directions of not-reheated clasts (our type A) are fully random, whereas those of reheated clasts (type B) are dispersed around a significant direction.

2) sampling PDC deposits at distal sites is different to the usual palaeomagnetic sampling. At the palaeomagnetic site level, the rock type shows little to no variations: oversampling is thus easy and, besides thermal demagnetization, many magnetic measurements are made for a sound investigation of the magnetic mineralogy, which results in a better understanding of the remanent magnetization of the rock. At distal sites, the small clasts, even a few millimeters in size, and their heterogenous rock types prevents a sound investigation of the magnetic mineralogy. Each clast is a single sample: its rock type and magnetic properties differ from those of the companion clast from the site. A site thus consists of clasts whose thermal history, lithology, magnetic characteristics, syn- or post-eruptive chemical alteration may show large variations and affect the precision of the reheating temperature value as given by the magnetic technique. In our experience, the precision of a few °C as in the case of archaeological remains (Cioni *et al.* 2004) – a case fully consistent with the model outlined in the previous section – is not achievable for lithic clasts. Our approach is therefore to give less weight to the precision of the reheating temperature of individual clasts and more to the accuracy of the deposition temperature value at the site. The procedure is described in Cioni et al. (2004) and summarized in the diagrams in Fig. 4: the reheating temperatures of individual clasts are evaluated taking into account any possible uncertainty, which often results in large temperature ranges; the deposition temperature is a common event that affected all clasts in a site and thus corresponds to the overlap of the individual temperature ranges.

Fig. 4 shows that most clasts concur to define the overlap range; the few outliers reasonably correspond to peculiar thermal history and/or magnetic characteristics.

Discussion

10

Irrespective of whether they are concentrated or diluted, it is evident that T_{dep} of PDCs from Somma-Vesuvius records lower values (maximum T_{dep} up to 420°C) with respect to eruptive temperature (assessed in the range 800-1000 °C; Santacroce *et al.* 2008). An important drop in temperature probably happen at the top of the gas thrust region and in the collapsing fountain. In addition, for these "small scale" PDCs, local variations in temperature happen due to physical processes that will be discussed below.

The starting point for the discussion is Figure 6, which reports all the T_{dep} of the PDC deposits emplaced in the last 22 kyr at Somma-Vesuvius. The deposits have been divided according to the main facies recognized in the field: massive, stratified, and fall. For each eruption, the main eruptive parameters are reported in Table 1, whereas the temperature variations for each deposit, along with the eruptive processes and the parent PDC characteristics, are shown in Table 3. For comparison, a few temperatures measured on the 79 AD eruption Plinian fallout are reported as well (Fig. 6). Although some eruptions have more data than others, some general comments can be provided from the inspection of Figure 6:

1. the 79 AD deposits (both stratified and massive) studied in the Pompeii excavations show the lowest temperatures values, down to 100 °C, and the largest temperatures range, which overlaps those of fall deposits;

2. apart from the 79 AD deposits in the excavated areas, all the eruption deposits show narrow temperature ranges, with average values of 300-330 for Avellino, Pompei and Pollena, and 360-380 °C for Pomici di Base, Greenish, Mercato and 1631;

3. the deposits of the 79 AD and Avellino eruption, sampled at 15 km away from the vent, do not show variations in temperature with distance;

4. the massive deposits of Mercato PDCs record the highest temperatures;

5. T_{dep} is independent of the deposit facies.

Based on this evidence, we will now discuss the observed temperature variations taking into account each of the possible factors that can influence the acquisition of the final values of T_{dep}.

Temperature and chemistry of the magma

The eruptive temperatures of the different magmas range from 850 °C, for the more evolved magmas, up to 1000 °C for the less evolved products (Table 1) (Cioni *et al.* 1999). Although most of the Somma-Vesuvius eruptions are chemically stratified, the composition-dependent variations in the temperature during the same eruption proved to be minor (Santacroce *et al.* 2008). Because the most evolved magma of Mercato is related to the hottest deposits, it is possible to infer that magma temperature does not make the main difference in final T_{dep}.

11

Intensity of the eruption (VEI)

We consider here only the peak intensity of Somma-Vesuvius eruptions, which is the only published data for the considered events. In this light, the intensity parameter is only a broad measure of energy released at a certain time of the eruption. Theoretically, a higher intensity of the eruption results in powerful columns, with more efficient air entrapment into the rising mixture. This may produce a lower T_{dep} of the pyroclastic material. Nevertheless, this simple relation is commonly complicated by other physical parameters, such as grain-size distribution, and mass partition within the column. Based on these considerations, is not surprising that deposit temperatures reported in Table 3 do not show any relation to the intensity of the eruption.

Magmatic versus phreatomagmatic activity

Although it is well known that water-magma interaction can be one of the most efficient ways to reduce the temperature of the erupting cloud (heat capacity of water is double that of air; Koyaguchi & Woods 1996), the phreatomagmatic deposits do not show any appreciable variation in T_{dep} with respect to their magmatic counterparts (Table 1). Only a few phreatomagmatic deposits in the 79 AD eruption show significant drops in temperature (Cioni *et al.* 2004). In contrast, in both the Pollena and Avellino phreatomagmatic deposits, the estimated T_{dep} does not show any significant reduction with respect to that of the magmatic ones. In order to explain the similar temperatures in magmatic and phreatomagmatic PDC deposits of the Pollena eruption, Zanella *et al.* (2008) suggested that the cooling effect of any water involved in the eruption was not sufficient to significantly reduce the temperature of the eruptive mixture. In the Avellino phreatomagmatic PDCs, Di Vito *et al.* (2009) adduced the increase of fine-grained juvenile material content as responsible for the increase of the heat-carrier (i.e. the magma) specific surface area, which enhanced its capability to transmit heat to the colder components of the pyroclastic mixture and to the entrapped ambient air. The presence of abundant fine particles lowers the porosity of the deposits, so for any fluid is more difficult to escape, consequently the thermal advection exchange of the deposit with the ambient is reduced.

This is an efficient mechanism of heat transfer when the current comprises mainly ash-grade fragments thermally and mechanically coupled with the surrounding gas (Cioni *et al.* 2004).

Grain-size

In PDC deposits from both Pollena and Pompeii eruptions, we found that local variations in temperatures by a few tens of °C can be observed between coarse-grained, fines-poor deposits and

their fine-grained counterparts. Usually the former show lower T_{dep} than the latter (Cioni *et al.* 2004; Zanella *et al.* 2007). Because efficiency of heat exchange in a PDC deposit is proportional to the surface area of juvenile fragments (the heat sources), the abundance of fine juvenile fractions results in a more efficient process of heat transfer to the colder lithic fragments than in the coarse-grained part of the deposit.

It appears that this process can balance the cooling effect due to heat consumption during phretomagmatic fragmentation, which produces abundant fines, as observed in the cases of Avellino, 79 AD and Pollena phreatomagmatic PDC deposits (Table 1).

Lithic content

The amount of cool lithic fragments entrapped in the flowing mixture was thought to be crucial in determining the temperature of the PDC at any time and the final T_{dep} (Marti *et al.* 1991).

Lithic fragments can be entrained in the eruptive mixture at different times, from the magma chamber walls, along the conduit due to erosion of wall rocks, at vent during crater erosion, or during flow of the PDC. The initial temperature of the fragments depends on their source location, and can be close to the magmatic temperature for lithic fragments from the magma chamber or the conduit walls, or ambient temperature for those entrained during PDC flow. The cooling effect also depends on the size of the entrained material, where only lithic clasts with radius less than 2 cm will reach thermal equilibrium with the parental flow before deposition (Cioni *et al.* 2004). The PDC deposits at Somma-Vesuvius contain variable amounts of lithic fragments, which can differ greatly even in PDCs from the same eruption (Table 1), but the different contents are not correlated with trends in T_{dep}. Thus, although there is evidence that entrainment of high volumes of cold lithic fragments can enhance cooling of a hot PDC (e.g. Eichelberger & Koch 1979), we find no evidence for significant lithic-induced cooling in Somma-Vesuvius PDCs.

Mechanisms of PDC generation (total collapse vs. marginal instability of the convective column vs. collapsing fountain)

Most of the PDCs from Somma-Vesuvius were generated by gravitational collapse of the erupting pyroclastic mixture. The height and style of collapse can potentially be one of the most important factors influencing the heat loss of the pyroclastic mixture. However, very little is known about the physical processes that act during partial or total collapse of pyroclastic columns and fountains, especially about the amount of air ingested during fall. This makes it difficult to have a precise assessment on the influence of collapsing behaviour on final T_{dep}. Nevertheless, although the absolute value of cooling is not evaluable, the relative difference between total and fountain

collapse appears to be negligible. This is because the height of collapse for these styles can be considered similar (within the gas thrust zone, a few hundred of meters in height), and the time of collapse is a few seconds, reducing the possibility to have great differences in cooling rate of the collapsing pyroclastic mixture. An exception might be boiling-over activity, which is described as an overspill of the crater rim, possibly without any clear established fountain (Cas & Wright, 1987). Among the Somma-Vesuvius deposits considered in this study only the massive PDCs from AD 1631 eruption and the EU3pfL at the end of the 79 AD magmatic phase (Table 1, Cioni *et al.* 2004, Shea *et al.* 2011, 2012), are from boiling over activity (Rosi *et al.* 1993), and they do not show any significant difference in T_{dep} with respect to the stratified deposits from the same eruptions (Fig. 6). In contrast, the two deposits emplaced by partial collapses, recognized in the 79 AD eruption, show the lowest temperature (220-280 °C, Table 1) for any of the products of the magmatic phase of the eruption. These low temperatures are related to a low initial temperature of the current, representing detachment and collapse of the marginal, fines-rich portions of the eruptive column, where turbulent ingestion of air was high (Cioni *et al.* 2004). It seems that in between all the different collapsing style, only the partial collapses are the ones able to produce cooler PDC deposits.

Massive versus stratified deposits

Figure 6 shows that the different facies of PDC deposits examined at Somma-Vesuvius have no clear correlation with the T_{dep}. PDCs are tipically density stratified and comprise an upper more diluted part and a lower, denser part (Valentine 1987; Sulpizio & Dellino 2008). The upper, diluted part is usually more turbulent than the basal part (the underflow), in which high particle concentration inhibits or reduces the development of turbulence. This implies that the upper and lower parts of a PDC can experience different cooling rates and amount of air entrainment during motion. Because of the cm-size (2-3 cm) of most of the analyzed lithic clasts, they cannot be transported for long time in the upper, more diluted part of the PDCs supported by turbulence (Dellino et al. 2008). This is shown by the common fine-grain size of the normally graded, massive facies indicative of deposition directly from the turbulent suspension. This means that, irrespective of whether they are in a diluted or concentrated PDC, they pass most of their travel time in the more concentrated underflow, where cooling due to ingestion of ambient air is reduced.

Such a behaviour can account for the similarity in T_{dep} between stratified and massive facies of PDC deposits (Table 1; Fig. 6). The temperatures measured in lithic clasts from fall deposits support this inference, being significantly lower than in PDC deposits (Table 1; Fig. 6).

The PDC deposits at Pompeii excavations are an apparent exception. However, inspection of the data in Table 1 shows that the lowest values are related to local increase in turbulence in EU3pf and

EU4pf (Gurioli *et al.* 2005, 2007) and general low temperature for EU7 and EU8 PDC deposits (Table 1). These latter units are representative of deposition from very diluted PDCs dominated by direct fallout or traction-dominated depositional regimes, in which turbulence and air ingestion were probably very effective.

However, in general, as already stated, for all the PDCs at Vesuvius, the loss of magmatic heat mostly occurred in the eruption column rather then in lateral flow, as also supported by the low temperature data from the fallout, in which most of the heat is lost (Fig. 6).

Travel distance

For the three eruptions, Avellino, Pompeii (excluding the Pompeii excavations) and Pollena, in which we could collect thin, fine-grained samples at medial-distal locations, we found values of T_{dep} not significantly different from proximal values (Table 1), a behaviour also observed in Taupo deposits (McClelland *et al.* 2004). This indicates that heat carriers in these PDC deposits were still thermally and mechanically coupled with the surrounding hot gas (Cioni *et al.* 2004; Di Vito *et al.* 2009). A reduced air entrainment may account for the limited heat loss from proximal to distal sites. Some of the data from Pompeii excavations make an exception (Gurioli *et al.* 2005; 2007; Zanella *et al.* 2007), but their behaviour is more related to depositional regime than to the distance travelled.

Thickness

Data from Table 1 show that the thicknesses of PDC deposits are not correlated to the final T_{dep}. Although some variations (of the orders of 20-40 °C) were found in the 79 AD deposits, that could be explained with increase in thickness (Cioni *et al.* 2004), the same findings were not proved in thick deposits studied within the eruption of Pollena (Zanella *et al.* 2008). This indicates that other physical parameters are more prominent in determining the heat exchange between heat carriers and cold lithic clasts than the thickness, at least for deposits from small to medium volume PDCs.

Conclusions

Despite the contrasting sedimentological features of the Somma-Vesuvius PDC deposits, the deposition temperatures mainly fall in the range 250-370 °C, with extreme values extending to around 100 °C and 420 °C. The lower range of T_{dep} between 100 °C and 250 °C characterises deposits from Pompeii excavations or from fall, indicating the fundamental importance of entrapment of cold ambient air into the moving pyroclastic mixture for lowering its internal tempearature. The 250-420 °C T_{dep} range shows a cluster between 270 °C and 370 °C, and contains all the deposits (both massive and stratified) from the slopes of Somma-Vesuvius. The clustering of

most of T_{dep} of deposits from Somma-Vesuvius slopes in a 100 °C range suggests similarity in boundary conditions during thermal equilibration of lithic clasts and pyroclastic mixture.

This is probably the result of the rapid development of non-turbulent underflow in which cooling was minimal. The high lithic clast content of some deposits also did not play a major role in decreasing T_{dep}. In the same way, the deposit thickness, travel distance, temperature and chemistry of the magma, mechanism of collapse (total, fountaning or boiling over) of the pyroclastic mixture and intensity of the eruption do not significantly correlate with the final T_{dep}. The only exception are some measurements on partial collapses deposits of the 79 AD, that show very low values of T_{dep}, in agreement with more ingestion of air in the marginal portions of the column. However, more measurements needs to be made, to make the statistic more robust, and the findings more general. Apparently, fragmentation behaviour also does not correlate with the T_{dep}, as the values from phreatomagmatic and magmatic deposits indistinguishable. This is because the heat consumed in thermohydraulic explosions (that reduce the available heat in the system) is balanced by the fine comminution of heat carrier particles (juvenile), which increases the heat-exchanging surface and makes the heat transfer more efficient. At equal boundary and initial conditions, the most effective process able to significantly cool down the T_{dep} of Somma-Vesuvius PDCs seems to be the ability to incorporate ambient air. In particular, the amount of cold air entrapped (and consequent heat loss) depending on the combined effect of turbulence of the moving flow and duration of transportation.

The significantly lower T_{deps} shown by fall and distal ash deposits of Pompeii eruption dominated by direct fallout regime testify for this hypothesis. Particles of fall deposits experience the same transportation of part of the fragments in a PDC (i.e. those supported by turbulence). For clast-size of around 2 cm, the travel time in the column and umbrella system is probably longer than those in a PDC, but not so long to completely cool down the lithic fragments of this size. This is an argument supporting the cooling due to ingestion of ambient air (e.g. due to turbulence), which is more effective in eruptive column and umbrella clouds. At the same, it supports the speculation that clasts of around 2 cm in size cool down mostly during fountain/collumn collapse, and that after collapse they have few chances to be cooled down by turbulence within a PDC, because they pass most of their travel time in the non-turbulent, basal part of the currents.

These results are of crucial importance when dealing with volcanic hazard assessment of one of the most dangerous volcanoes in the world, beacause they indicate how PDCs at Somma-Vesuvius have emplacement temperatures always above the threshold of danger for human life, irrespective of their transport and depositional regime.

References

Aramaki, S. & Akimoto, S. 1957. Temperature estimation of pyroclastic deposits by natural remanent magnetism. *American Journal of Science*, **255**, 619-627.

Bardot, L. & McClelland, E. 2000. The reliability of emplacement temperature estimates using palaeomagentic methods: a case study from Santorini, Greece. *Geophysical Journal International*, **143**, 39-51.

Baxter, P.J., Neri, A. & Todesco, M. 1998. Physical modeling and human survival in pyroclastic flows. *Natural Hazard*, **17**, 163-176.

Baxter, P.J., Aspinall, W.P., Neri, A., Zuccaro, G., Spence, R.J.S., Cioni, R. & Woo, G. 2008. Emergency planning and mitigation at Vesuvius: a new evidence-based approach. *Journal of Volcanology and Geothermal Research*, **178**, 454-473.

Bertagnini, A., Landi, P., Rosi, M. & Vigliargio, A. 1998. The Pomici di Base plinian eruption of Somma-Vesuvius. *Journal of Volcanology and Geothermal Research*, **83**, 219-239.

Branney, M.J. & Kokelaar, P. 2002. Pyroclastic density currents and the sedimentation of ignimbrites. *Geological Society of London*, Memoir 27, 1–143.

Cafarella, L., De Santis, A. & Meloni, A. 1992. *Il catalogo geomagnetico storico italiano*. Istituto Nazionale di Geofisica, Roma, Italy.

Chadwick, R.A. 1971. Paleomagnetic criteria for volcanic breccia emplacement. *Geological Society of America Bulletin*, **82**, 2285-2294.

Cioni, R., Marianelli, P. & Santacroce, R. 1999. Temperatures of Vesuvius magmas. *Geology*, **27**, 443-446

Cioni, R., Sulpizio, R. & Garruccio, N. 2003. Variability of the eruption dynamics during a Subplinian event: the Greenish Pumice eruption of Somma-Vesuvius (Italy). *Journal of Volcanology and Geothermal Research*, **124**, 89-114.

Cioni, R., Gurioli, L., Lanza, R. & Zanella, E. 2004. Temperatures of A.D. 79 pyroclastic density current deposits (Vesuvius, Italy). *Journal of Geophysical Research*, **109**, B02207, doi:10.1029/2002JB002251.

Cioni, R., Bertagnini, A., Santacroce, R. & Andronico, D. 2008. Explosive activity and eruption scenarios at Somma-Vesuvius (Italy): towards a new classification scheme. *Journal of Volcanology and Geothermal Research*, **178**, 331-346.

Di Vito, M.A., Zanella, E., Gurioli, L., Lanza, R., Sulpizio, R., Bishop, J., Tema, E., Boenzi, G. & Laforgia, E. 2009. The Afragola settlement near Vesuvius, Italy: The destruction and abandonment of a Bronze Age village revealed by archaeology, volcanology and rock-magnetism. *Earth and Planetary Science Letters*, **277**, 408-421, doi:10.1016/j.epsl.2008.11.006.

Dobran, F., Neri, A. & Todesco, M. 1994. Assessing the pyroclastic flow hazard at Vesuvius. *Nature*, **367**, 551-554.

Downey, W.S. & Tarling, D.H. 1984. Archaeomagnetic Dating of Santorini Volcanic-Eruptions and Fired Destruction Levels of Late Minoan Civilization. *Nature*, **309**, 519-523.

Druitt, T.H. 1998. Pyroclastic density currents. *In*: Gilbert, J.S., Sparks, R.S.J. (eds) *The physics of esplosive volcanic eruptions*. Geological Society, London, Special Publications 145, 21, 145-182.

Eichelberger, J.C. & Koch, F.G. 1979. Lithic fragments in the Bandelier tuff, Jemez Mountains, New Mexico. *Journal of Volcanology and Geothermal Research*, **5**, 115–134

Esposti-Ongaro, T., Neri, A., Todesco, M. & Macedonio, G. 2002. Pyroclastic flow hazard assessment at Vesuvius (Italy) by using numerical modelling. 2. Analysis of flow variables. *Bulletin of Volcanology*, **64**, 155-177.

Esposti-Ongaro, T., Neri, A., Menconi, G., de'Michieli Vitturi, M., Marianelli, P., Cavazzoni, C., Erbacci, G. & Baxter, P.J. 2008. Transient 3D numerical simulations of column collapse and pyroclastic density current scenarios at Vesuvius, *Journal of Volcanology and Geothermal Research*, **3/178**, doi:10.1016/j.jvolgeores.2008.06.036.

Fisher, R.A. 1953. Dispersion on a sphere. *Proceedings of the Royal Society*, **217**, 295–305.

Gurioli, L., Cioni, R., Sbrana, A. & Zanella, E. 2002. Transport and deposition from pyroclastic flows over densely inhabited areas: Herculaneum (Italy). *Sedimentology*, **46**, 1–26.

Gurioli, L., Pareschi, M.T., Zanella, E., Lanza, R., Deluca, E. & Bisson, M. 2005. Interaction of pyroclastic density currents with human settlements: Evidence from ancient Pompeii. *Geology*, **33**, 441-444, doi: 10.1130/G21294.1.

Gurioli, L., Zanella, E., Pareschi, M.T. & Lanza, R. 2007. Influences of urban fabric on pyroclastic density currents at Pompeii (Italy): 1. Flow direction and deposition. *Journal of Geophysical Research*, **112**, B05213, doi:10.1029/2006JB004444.

Gurioli, L., Sulpizio, R., Cioni, R., Sbrana, A., Santacroce, R., Luperini, W. & Andronico, D. 2010. Pyroclastic flow hazard assessment at Somma-Vesuvius based on the geological record. *Bulletin of Volcanology*, **72**, 1021-1038.

Halls, H.C. 1978. The use of converging remagnetization circles in paleomagnetism. *Physics of the Earth and Planetary Interiors*, **16**, 1-11.

Hoblitt, R.P. & Kellogg, K.S. 1979. Emplacement temperatures of unsorted and unstratified deposits of volcanic rcok debris as determined by paleomagnetic techniques. *Geological Society of America Bulletin*, **90**, 633-642.

James, D.W., 1968. The thermal diffusivity of ice and water between −40 and +60 °C. *Journal of Mathematical Science*, 540–543.

Kent, D.V., Ninkovich, D., Pescatore, T. & Sparks, R.S.J. 1981. Paleomagnetic determination of emplacement temperature of Vesuvius AD 79 pyroclastic deposits. *Nature*, **290**, 393-396.

Koyaguchi, T. & Woods, A.W. 1996. On the explosive interaction of water and magma. *Journal of Geophysical Research*, **101**, 5561-5574.

Marti, J., Diez-Gil, L. & Ortiz, R. 1991 Conduction model for the thermal influence of lithic clasts in mixtures of hot gases and ejecta. *Journal of Geophysical Research*, **96**, 21879–21885.

McClelland, E. 1996. Theory of CRM acquired by grain growth, and its application for TRM discrimination and paleointensity determination in igneous rocks. Geophysical Journal International, 126, 271-280.

McClelland, E., Wilson, C.J.N. & Bardot, L. 2004. Palaeotemperature determinations for the 1.8-ka Taupo ignimbrite, New Zealand, and implications for the emplacement history of a high-velocity pyroclastic flow. *Bulletin of Volcanology*, **66**, 492-513. doi:10.1007/s00445-003-0335-5

McFadden, P.L. & McElhinny, M.W. 1988. The combined analysis of remagnetization circles and direct observations in palaeomagnetism. *Earth and Planetary Science Letters*, **87**, 161–172.

Mele, D., Sulpizio, R,, Dellino, P. & La Volpe, L. 2011. Stratigraphy and eruptive dynamics of a pulsating Plinian eruption of Somma-Vesuvius: the Pomici di Mercato (8900 years B.P.). *Bulletin of Volcanology*, doi: 10.1007/s00445-010-0407-2.

Noel, M. & Batt, C.M. 1990. A method for correcting geographically separated remanence directions for the purpose of archaeomagnetic dating. *Geophysical Journal International*, **102**, 753-756.

Paterson, G.A., Roberts, A.P., Mac Niocaill, C., Muxworthy, A.R., Gurioli, L., Viramonté, J.G., Navarro, C. & Weider, S. 2010. Paleomagnetic determination of emplacement temperatures of pyroclastic deposits: an under-utilized tool. *Bulletin of Volcanology*, 79, 309-330. doi:10.1007/s00445-009-0324-4.

Rosi, M. & Santacroce, R. 1983. The A.D. 472 "Pollena" eruption: volcanological and petrological data for this poorly-known, Plinian-type event at Vesuvius. Journal of Volcanology and Geothermal Research, 17, 249–271.

Rosi, M., Principe, C. & Vecci, R. 1993. The 1631 Vesuvius eruption. A reconstruction based on historical and stratigraphical data. *Journal of Volcanology and Geothermal Research*, **58**, 151-182.

Rossano, S., Mastrolorenzo, G. & De Natale, G. 1998. Computer simulations of pyroclastic flows on Somma-Vesuvius volcano. *Journal of Volcanology and Geothermal Research*, **82**, 113-137.

Santacroce, R. (Ed.) 1987. *Somma-Vesuvius*. In: Quaderni de "La Ricerca Scientifica", 114. CNR, Rome.

Santacroce, R., Cioni, R., Marianelli, P., Sbrana, A., Sulpizio, R., Zanchetta, G., Donahhue, D.J. & Joron, J.L. 2008. Age and whole rock–glass compositions of proximal pyroclastics from the major explosive eruptions of Somma-Vesuvius: A review as a tool for distal tephrostratigraphy. *Journal of Volcanology and Geothermal Research*, **177**, 1-18.

Shea, T., Gurioli, L., Houghton, B.F, Cioni, R., & Cashman, K.V. 2011. Transition from stable to collapsing column during the 79AD eruption of Vesuvius: the role of pyroclats density. *Geology* doi:10.1130/G32092.1

Shea, T., Gurioli, L. & Houghton, B.F. 2012. Transitions between fall phases and pyroclastic density currents during the AD 79 eruption at Vesuvius: building a transient conduit model from the textural and volatile record *Bulletin of Volcanology* **74**, 2363–2381.

Sulpizio, R., Mele, D., Dellino, P. & La Volpe, L. 2005. A complex Subplinian-type eruption from low viscosity, phonolitic to tephri-phonolitic magma: the AD 472 (Pollena) eruption of Somma-Vesuvius, Italy. *Bulletin of Volcanology*, doi: 10.1007/s00445-005-0414-x

Sulpizio, R, Mele, D., Dellino, P. & La Volpe, L, 2007. Deposits and physical properties of pyroclastic density currents during complex Subplinian eruptions: the AD 472 (Pollena) eruption of Somma-Vesuvius, Italy. *Sedimentology*, 1-29, doi: 10.1111/j.1365-3091.2006.00852.x

Sulpizio, R., Bonasia, R., Dellino, P., Di Vito, M.A., La Volpe, L., Mele, D., Zanchetta, G. & Sadori, L. 2008. Discriminating the long distance dispersal of fine ash from sustained columns or near ground ash clouds: The example of the Pomici di Avellino eruption (Somma-Vesuvius, Italy). *Journal of Volcanology and Geothermal Research*, **177**; 263-276,

Sulpizio R. & Dellino, P. 2008. Chapter 2 Sedimentology, Depositional Mechanisms and Pulsating Behaviour of Pyroclastic Density Currents. *Developments in Volcanology*, **10**, 57-96.

Sulpizio, R., Bonasia, R., Dellino, P., Mele, D., Di Vito, M.A. & La Volpe, L. 2010. The Pomici di Avellino eruption of Somma-Vesuvius (3.9 Ka Bp). Part II: Sedimentology and Physical Volcanology of Pyroclastic Density Current Deposits. *Bulletin of Volcanology*, doi: 10.1007/S00445-009-0340-4

Sulpizio, R., Cioni, R., Di Vito, A., Mele, D., Bonasia, R. & Dellino, P., 2010. The Pomici di Avellino eruption Of Somma-Vesuvius (3.9 Ka Bp). Part I: Stratigraphy, Compositional Variability and Eruptive Dynamics. *Bulletin of Volcanology*, doi: 10.1007/S00445-009-0339-X

Tanguy, J.C., Le Goff, M., Principe, C., Arrighi, S., Chillemi, V., Paiotti, A., La Delfa, S. & Patanè G. 2003. Archeomagnetic dating of Mediterranean volcanics of the last 2100 years: validity and limits. *Earth and Planetary Science Letters*, **211**, 111-124, doi:10.1016/S0012-821X(03)00186-9.

Tilling, R.I. & Lipman, P.W. 1993. Lessons in reducing volcano risk, *Nature*, **364**, 277-280.

Valentine, G.A. 1997. Damage to structures by pyroclastic rocks and surges, inferred from nuclear weapons effects. Jounal of Volcanology and Geothermal Research, 87, 117-140.

Velinov, T.S., Bransalov, K. & Mihovski, M., 1993. A thermal diffusion study of the solid phase of porous samples. *Measurement Science and Technology*. 4, 1266–1268.

Vosteen, H.D. & Schellschmidt, R., 2003. Influence of temperature on thermal conductivity, thermal capacity and thermal diffusivity for different types of rock. *Physics and Chemistry of the Earth*, 28, 449-509.

Zanchetta, G., Sulpizio, R., Roberts, N., Cioni, R., Eastwood, W. J., Siani, G., Paterne, M., Santacroce, R. 2011. Tephrostratigraphy, chronology and climatic events of the Mediterranean basin during the Holocene: an overview. *The Holocene*, 21, 33-52. doi:10.1177/0959683610377531

Zanella, E., Gurioli, L., Chiari, G., Ciarallo, A., Cioni, R., De Carolis, E. & Lanza, R. 2000. Archaeomagnetic results from mural paintings and pyroclastic rocksin Pomepii and Herculaneum. *Physics of the Earth and Planetary Interiors*, **118**, 227-240.

Zanella, E., Gurioli, L., Pareschi, M.T. 6 Lanza, R. 2007. Influences of urban fabric on pyroclastic density currents at Pompeii (Italy), part II: temperature of the deposits and hazard implication. *Journal of Geophysical Research*, **112**, B05214, doi:10.1029/2006JB004775.

Zanella, E., Gurioli, L., Lanza, R., Sulpizio, R. & Bontempi, M 2008. Deposition temperature of the AD 472 Pollena pyroclastic density currents deposits, Somma-Vesuvius, Italy. *Bulletin of Volcanology*, **70**, 1237-1248, doi:10.1007/s00445-008-0199-9.

Zuccaro, G., Cacace, F., Spence, R.J.S. & Baxter, P.J. 2008. Impact of explosive eruption scenarios at Vesuvius. *Journal of Volcanology and Geothermal Research*, **178**, 416–453.

Zijderveld, J.D.A. 1967. AC demagentization of rocks: analysis of results. In: Runcorn S.K., Creer, K.M. & Collinson, D.W. (eds). Method in paleomagnetism. Elsevier, Amsterdam, 254-286.
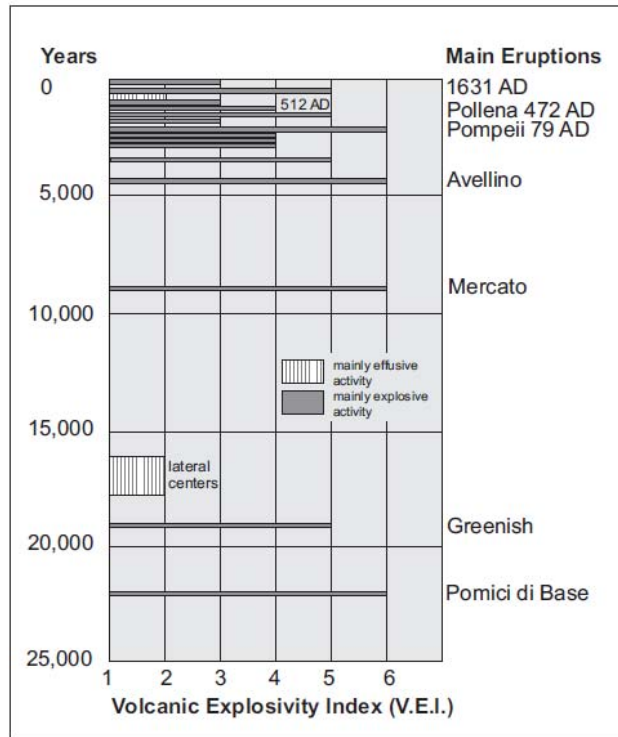
Fig. 1 - Main explosive eruptions of Somma-Vesuvius.
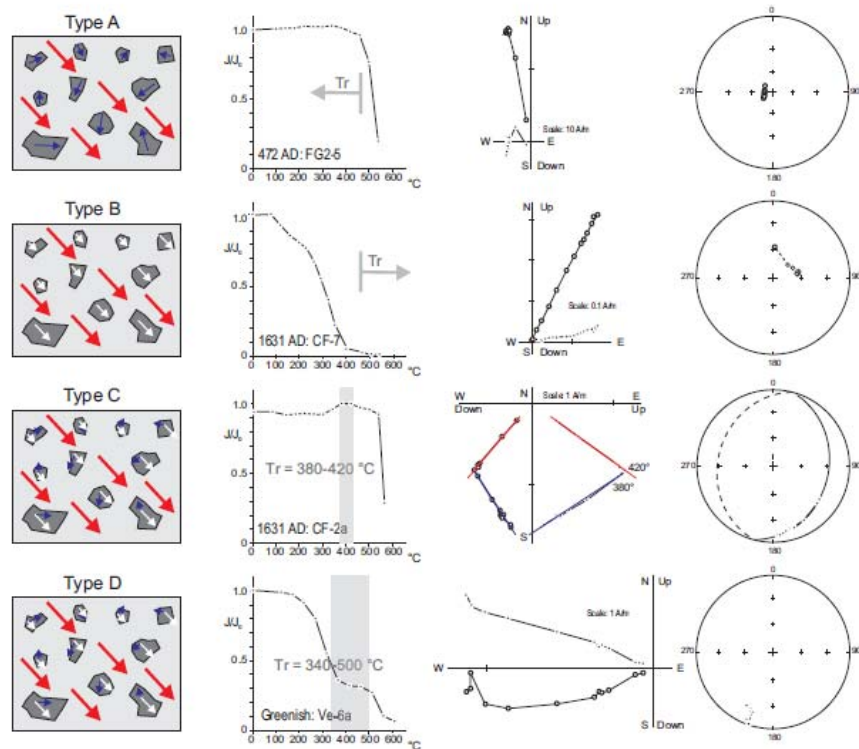
Fig. 2 - Clasts behaviour during stepwise thermal demagnetization. Columns (left to rigth):
1) clast type A, B, C, D (Cioni *et al*. 2004). Arrows: red = TRM of the fine-grained matrix, coinciding with the ambient magnetic field at the time of eruption; blue = primary TRM acquired when the clast formed; white= secondary TRM acquired when the clast cooled within the deposit. 2) normalized intensity decay curve. The grey bar shows the re-heating range. 3) Zijderveld (1967) diagram: solid/open dot = declination/apparent inclination; figures = T value (°C). 4) equal-area projection: solid/open dots = lower/upper hemisphere.
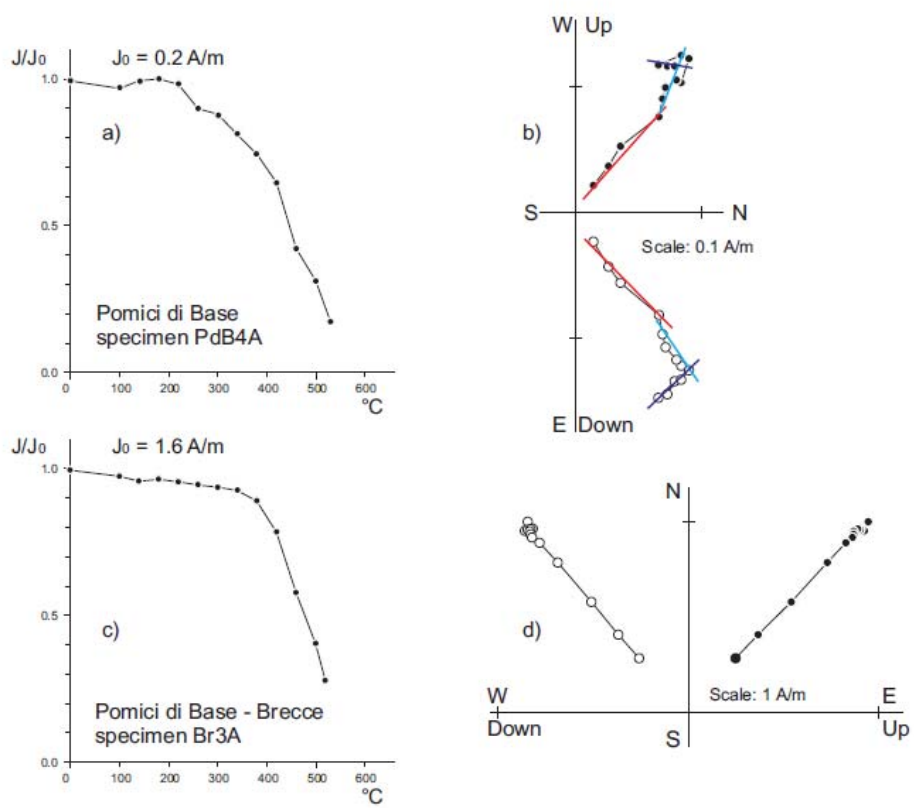
Fig. 3 - Examples of thermal demagnetization of lithic clasts. Symbols as in Fig. 2.
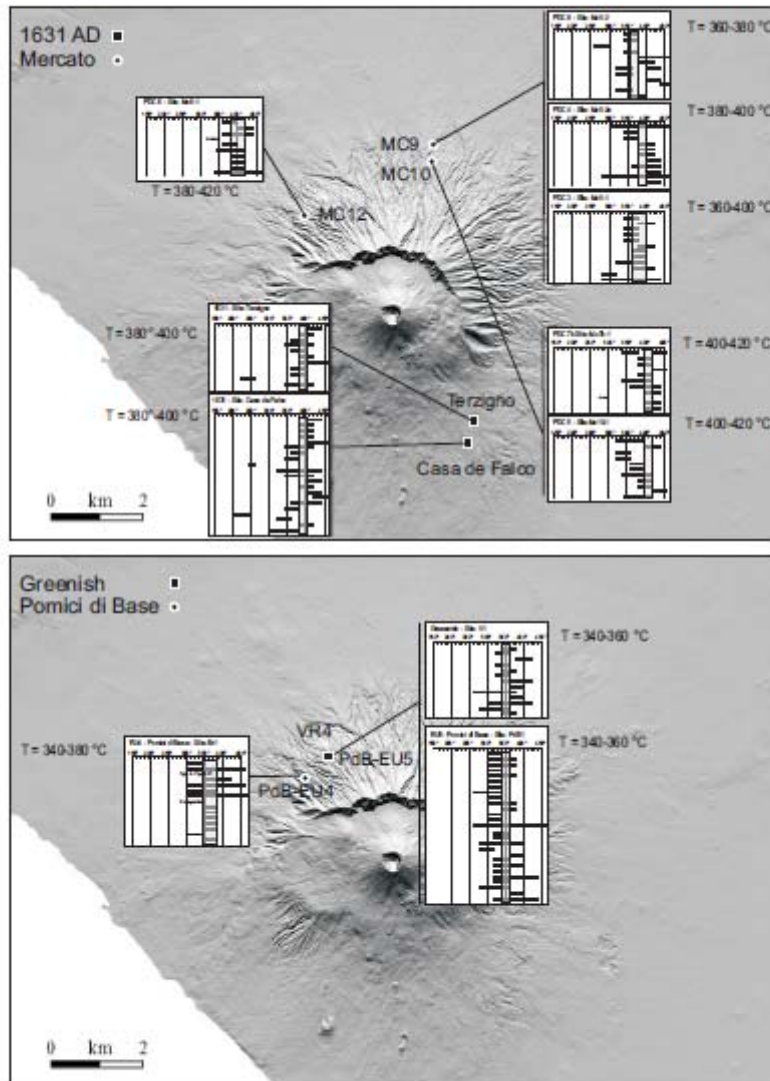
Fig. 4 - Digital elevation model (courtesy M.T. Pareschi) of Vesuvius and map of deposition temperature of the pyrocvlastic deposits of the Pomici di Base, Greenish, Mercato and AD1631 eruptions. The insets show the re-heating temperature (T_r) of all individual clasts and the overlap interval regarded as the deposition temperature (T_{dep}).

Fig. 5 - Equal-area projection of the secondary TRM direction in lithic clasts from the 1631 eruption deposits. Symbols: dot = clast ChRM direction; great circle = remagnetization circle; star = mean direction with 95% ellipse of confidence; diamond = AD 1631 direction from historical measurement.
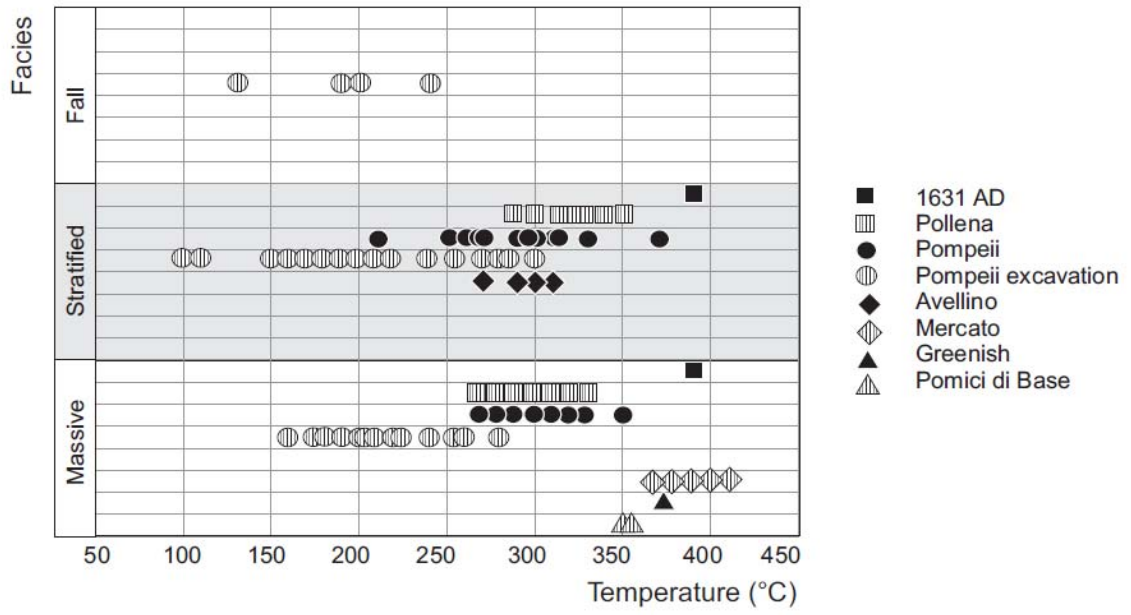
Fig. 6 - Deposition temperature vs. facies of the pyroclastic deposits of Somma-Vesuvius.

Table captions

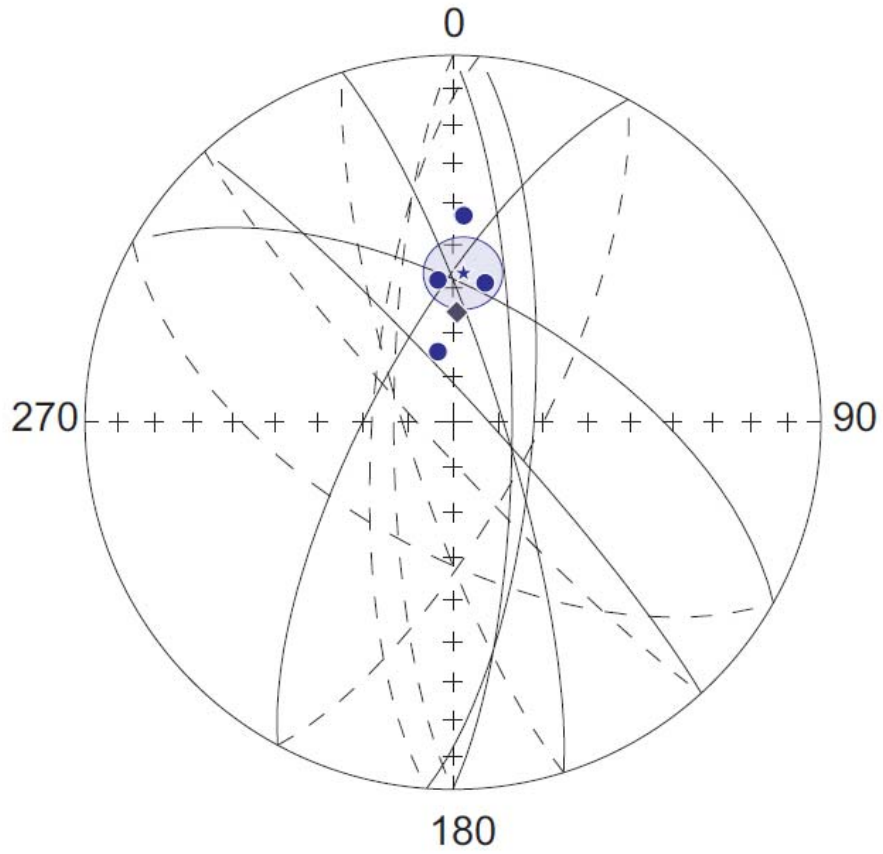| Eruption (Reference)	Unit	Site	D km	Eruptive processes	PDCs generation	Thickness cm	Grain size Mdφ	F1 %	Lithic content %	Facies	n/N	T_{dep} (°C)	Type % A	B	C	D
1631		Casa de Falco	5.5	Magmatic	collapsing fountain	250	--	-	--	massive	17/22	380-400	-	4	64	32
(this paper)		Terzigno	5.7	Magmatic	collapsing fountain	300	--	-	--	massive	10/11	380-400	-	-	55	45
Pollena	Fy2	Villa Sora	6.5	Phreatomagmatic	collapsing fountain	100	--	-	--	massive	8/10	260-280	-	-	40	60
(Zanella *et al.* 2008)	Fy1	Villa Sora	6.5	Phreatomagmatic	collapsing fountain	50	--	-	--	massive	10/10	280-300	-	-	40	10
	Fy	VS1	4.4	Phreatomagmatic	collapsing fountain	200	--	-	--	massive	10/12	260-300	-	-	34	66
		VS4	5.0	Phreatomagmatic	collapsing fountain	250	0.89	63	50	massive	11/12	300-320	-	-	55	50
		VS13	4.8	Phreatomagmatic	collapsing fountain	300	0.48	58	--	massive	5/5	260-280	-	-	40	60
	Sy	VS4	5.0	Phreatomagmatic	collapsing fountain	50	0.50	60	43	stratified	4/4	320-340	-	-	17	83
		VS4	5.0	Phreatomagmatic	collapsing fountain	50	0.50	39	52	stratified	6/6	280-300	-	-	7	83
		VS13	4.8	Phreatomagmatic	collapsing fountain	35	1.07	77	44	stratified	13/13	280-320	-	-	31	69
		VS23	6.9	Phreatomagmatic	collapsing fountain	10	--	-	--	stratified	4/4	300-320	-	-	55	50
	Fg2	VS13	4.8	Magmatic	total collapse	250	--	-	--	massive	14/14	260-300	7	-	43	50
	Fg1	VS13	4.8	Magmatic	total collapse	300	0.80	39	--	massive	8/8	260-300	-	-	63	37
		VS20a	2.9	Magmatic	total collapse	500	0.20	48	--	massive	12/13	260-300	-	-	31	69
		VS20b	3.0	Magmatic	total collapse	550	--	-	--	massive	10/12	300-340	-	-	42	58

Location	Unit	Sample		Magma	Eruptive style					Structure	T	T range (°C)				
		VS20c	3.2	Magmatic	total collapse	500	0.50	40	--	massive	10/13	300-320	-	-	46	54
		VS31	2.3	Magmatic	total collapse	300	--	-	--	massive	9/9	260-280	-	-	44	56
	S2	Pozzelle Quarry	5.5	Magmatic	total collapse	60	--	-	--	stratified	16/18	280-320	6	-	39	55
		VS2	4.8	Magmatic	total collapse	50	1.52	84	45	stratified	10/10	280-300	-	-	70	30
		VS14	8.4	Magmatic	total collapse	5	0.50	44	48	stratified	7/8	300-340	-	-	38	62
		VS23	6.9	Magmatic	total collapse	8	1.69	88	42	stratified	10/11	300-340	-	-	18	82
	Natop	Pozzelle Quarry	5.5	Magmatic	collapsing fountain	300	--	-	--	massive	15/16	300-340	-	6	25	69
	base	Pozzelle Quarry	5.5	Magmatic	collapsing fountain	300	--	-	--	massive	9/10	280-300	-	10	20	70
		VS5	2.4	Magmatic	collapsing fountain	250	0.90	37	36	massive	8/11	280-300	17	-	50	33
		VS6	2.7	Magmatic	collapsing fountain	80	1.10	31	39	massive	13/15	320-340	-	-	60	40
		VS20	3.0	Magmatic	collapsing fountain	150	0.92	69	41	massive	7/9	300-320	-	-	22	78
	S1	VS2	4.8	Magmatic	collapsing fountain	50	1.17	77	43	stratified	6/7	340-360	13	-	25	62
		VS6	2.7	Magmatic	collapsing fountain	20	0.71	70	39	stratified	7/7	320-340	-	-	43	57
		VS13	4.8	Magmatic	collapsing fountain	5	--	-	--	stratified	12/14	310-340	-	-	54	46
		VS17	3.0	Magmatic	collapsing fountain	50	0.49	60	44	stratified	6/7	320-360	-	-	57	43
	LRPF	VS5	2.4	Magmatic	side collapse	350	0.70	41	58	massive	12/15	280-320	-	-	53	47
Pompeii	EU8L	Pollena	4.6	Phreatomagmatic	collapsing fountain	300	1.00	30	39	massive, valley pond	10	280-310				
(Cioni *et al.* 2004)		Pollena	4.6	Phreatomagmatic	collapsing fountain	100	1.00	28	55	massive, valley pond	5	250-280				

Group	Locality		Magma type	Eruption style					Deposit		Elevation
	Traianello	5.0	Phreatomagmatic	collapsing fountain	600	--	-	--	massive, valley pond	9	280-320
	Ercolano	7.0	Phreatomagmatic	collapsing fountain	60	0.00	53	62	massive, valley pond	4	340-360
EU7	Cinque Vie	6.3	Phreatomagmatic	total collapse	69	2.00	65	--	stratified	5	180-240
EU6	Zabatta	4.8	Phreatomagmatic	total collapse	200	-2.00	27	--	massive, valley pond	14	280-300
EU4	Angri	5.0	Phreatomagmatic	total collapse	9	3.00	66	--	stratified	5	310-340
	Pompeii	9.5	Phreatomagmatic	total collapse	30	2.00	76	--	stratified	8	280-300
	Casa de Falco	6.2	Phreatomagmatic	total collapse	130	2.00	76	--	stratified	5	310-330
	Cava Molara	3.9	Phreatomagmatic	total collapse	200	0.00	70	--	stratified	6	300-340
	Terzigno	6.3	Phreatomagmatic	total collapse	67	1.00	61	--	stratified	1	300-340
	Cinque Vie	6.3	Phreatomagmatic	total collapse	200	--	-	--	stratified	7	280-300
	Villa Telesi	4.7	Phreatomagmatic	total collapse	60	2.00	88	--	stratified	5	260-300
	Lagno Macedonia	5.3	Phreatomagmatic	total collapse	34	--	-	--	stratified	4	290-310
	Volto Santo	4.0	Phreatomagmatic	total collapse	100	0.00	57	--	stratified	4	300-310
EU3 pf	Cava Molara	3.9	Magmatic	total collapse	150	1.00	50	--	stratified	7	300-320
	Terzigno	6.3	Magmatic	total collapse	30	0.50	56	--	stratified	12	340-360
	Ercolano	7.0	Magmatic	total collapse	250	-0.50	43	19	massive	8	360-380
	Ercolano	7.0	Magmatic	total collapse	150	-1.40	29	37	massive	12	320-340
	Traianello	5.0	Magmatic	total collapse	300	--	-	--	massive	8	240-280
	Traianello	5.0	Magmatic	total collapse	200	--	-	--	massive	6	260-280
	Pollena	4.6	Magmatic	total collapse	40	2.00	54	--	stratified	5	280-310

31

	top	Pollena	4.6	Magmatic	total collapse	40	1.00	56	--	stratified	3	250-280				
	base	Pollena	4.6	Magmatic	total collapse	40	1.00	-34	--	stratified	5	280-310				
	EU3 pfi	Terzigno	6.3	Magmatic	marginal instability	25	2.00	-4	--	stratified	5	220-280				
	EU2/3pf	Terzigno	6.3	Magmatic	marginal instability	10	0.00	50	--	stratified	3	220-280				
Pompeii excavation (Zanella *et al.* 2007) (Gurioli *et al.* 2007)	EU8	site 7a	9.5	Phreatomagmatic	collapsing fountain	60	2.00	78	--	stratified	5	180-220	-	-	20	80
		site 16	9.5	Phreatomagmatic	collapsing fountain	60	--	-	--	stratified	1	140-180	-	-	100	--
	EU7 II ash	site 1	9.5	Phreatomagmatic	total collapse	10	--	-	--	stratified	3	260-300	-	-	100	--
		site 2a	9.5	Phreatomagmatic	total collapse	11	--	-	--	stratified	6	200-240	-	-	50	50
		site 2c	9.5	Phreatomagmatic	total collapse	20	2.50	82	--	stratified	4	210-240	-	-	--	100
		site 7a	9.5	Phreatomagmatic	total collapse	19	--	-	--	stratified	7	200-240	-	-	29	71
		site 10	9.5	Phreatomagmatic	total collapse	26	1.25	63	--	stratified	4	200-210	-	-	25	75
		site 11	9.5	Phreatomagmatic	total collapse	16	3.03	79	--	stratified	6	200-220	-	-	50	50
		site 12c	9.5	Phreatomagmatic	total collapse	18	2.82	76	--	stratified	6	180-200	-	-	67	33
		site 14	9.5	Phreatomagmatic	total collapse	12	--	-	--	stratified	3	180-220	-	-	33	67
		site 22a	9.5	Phreatomagmatic	total collapse	11	2.58	81	--	stratified	5	220-260	-	-	40	60
		site 25	9.5	Phreatomagmatic	total collapse	11	--	-	--	stratified	6	180-200	-	-	100	--
		site 17b	9.5	Phreatomagmatic	total collapse	23	--	-	--	stratified	5	180-220	-	-	20	80
	EU7 I ash	site 2c	9.5	Phreatomagmatic	total collapse	20	2.50	82	--	stratified	5	210-240	-	-	60	40
		site 7a	9.5	Phreatomagmatic	total collapse	19	--	-	--	stratified	4	220-260	-	-	50	50
	EU4 pf	site 1	9.5	Phreatomagmatic	total	49	2.16	87	--	stratified	3	260-	-	-	33	67

Site		Type	Category					Structure		Depth				
		c	collapse							300				
site 2a	9.5	Phreatomagmatic	total collapse	215	2.66	89	--	stratified	7	200 / 240 / 260	-	-	71	29
site 2b	9.5	Phreatomagmatic	total collapse	360	0.92	44	--	stratified	1	260 / 300 / 280	-	-	00	--
site 2c	9.5	Phreatomagmatic	total collapse	159	1.34	45	--	stratified	14	290 / 240	-	-	55	50
site 5e	9.5	Phreatomagmatic	total collapse	110	3.03	81	--	stratified	5	240 / 270 / 270	-	-	46	00
site 5f	9.5	Phreatomagmatic	total collapse	190	1.59	29	--	stratified	5	270 / 300 / 240	-	-	46	00
site 6	9.5	Phreatomagmatic	total collapse	70	2.43	71	--	stratified	7	240 / 270 / 280	-	-	45	37
site 7a	9.5	Phreatomagmatic	total collapse	250	1.53	60	--	stratified	9	280 / 320 / 270	-	-	63	73
site 7b	9.5	Phreatomagmatic	total collapse	92	--	-	--	stratified	9	270 / 300 / 280	-	-	63	73
site 9	9.5	Phreatomagmatic	total collapse	153	--	-	--	stratified	11	280 / 300 / 180	-	-	54	55
site 10	9.5	Phreatomagmatic	total collapse	165	1.93	33	--	stratified	10	180 / 200 / 160	-	-	73	00
site 11	9.5	Phreatomagmatic	total collapse	90	0.52	45	--	stratified	14	140 / 180	-	-	00	--
site 12a	9.5	Phreatomagmatic	total collapse	170	0.65	55	--	stratified	12	140 / 160 / 100	-	-	81	37
site 12b	9.5	Phreatomagmatic	total collapse	160	--	-	--	stratified	6	100 / 120 / 160	-	-	36	37
site 12c	9.5	Phreatomagmatic	total collapse	95	1.68	62	--	stratified	8	160 / 200 / 140	-	-	55	00
site 13	9.5	Phreatomagmatic	total collapse	86	--	-	--	stratified	13	140 / 160 / 180	-	-	63	28
site 14	9.5	Phreatomagmatic	total collapse	95	1.80	61	--	stratified	3	180 / 220 / 220	-	-	--	00
site 21	9.5	Phreatomagmatic	total collapse	83	2.85	76	--	stratified	6	220 / 260 / 260	-	-	55	00
site 22a	9.5	Phreatomagmatic	total collapse	46	--	-	--	stratified	4	260 / 300 / 260	-	-	--	00
site 22b	9.5	Phreatomagmatic	total collapse	50	1.29	19	--	stratified	4	260 / 300 / 180	-	-	55	00
site 22c	9.5	Phreatomagmatic	total collapse	100	1.75	29	--	stratified	4	180 / 220	-	-	55	00

33

Formation	Unit	Site	No.	Type	Class					Structure		Range				
		site 25	9.5	Phreatomagmatic	total collapse	177	2.60	25	--	stratified	10	100-120	-	-	90	10
		site 16	9.5	Phreatomagmatic	total collapse	80	--	-	--	stratified	6	80-120	-	-	33	67
		site 18b	9.5	Phreatomagmatic	total collapse	70	--	-	--	stratified	7	200-220	-	-	29	71
		site 19a	9.5	Phreatomagmatic	total collapse	117	--	-	--	stratified	8	260-300	-	-	62	38
		site 19b	9.5	Phreatomagmatic	total collapse	107	--	-	--	stratified	6	260-280	-	-	50	50
	EU4 fall	site 13	9.5	Phreatomagmatic	fall	6	1.89	10	--	massive	4	220-260	-	-	25	75
	EU3 pf	site 1	9.5	Magmatic	total collapse	16	2.07	83	--	stratified	6	260-300	-	-	50	50
		site 2a	9.5	Magmatic	total collapse	13	2.33	86	--	stratified	8	240-280	-	-	62	38
		site 2b	9.5	Magmatic	total collapse	17	2.12	75	--	stratified	6	240-270	-	-	17	83
		site 7a	9.5	Magmatic	total collapse	30	1.17	60	--	stratified	5	260-300	-	-	40	60
		site 11	9.5	Magmatic	total collapse	18	2.23	77	--	stratified	6	200-210	-	-	67	33
		site 12a	9.5	Magmatic	total collapse	19	1.11	57	--	stratified	5	140-220	-	-	--	100
		site 13	9.5	Magmatic	total collapse	7	--	-	--	stratified	5	170-180	-	-	60	40
		site 14	9.5	Magmatic	total collapse	5	--	-	--	stratified	1	180-220	-	-	--	100
		site 22c	9.5	Magmatic	total collapse	20	0.63	56	--	stratified	4	220-260	-	-	50	50
		site 18a	9.5	Magmatic	total collapse	24	--	-	--	stratified	10	180-220	-	-	60	40
		site 18b	9.5	Magmatic	total collapse	24	--	-	--	stratified	2	180-220	-	-	--	100
	EU3 fall	site 17b	9.5	Magmatic	fall	160	--	-	--	massive	6	180-220	-	-	33	67
		site 21	9.5	Magmatic	fall	160	3.23	3	--	massive	6	180-200	-	-	67	33
	EU2 fall	site 15	9.5	Magmatic	fall	140	3.18	3	--	massive	2	120-140	-	-	100	--
Avellino	EU5	Volto	4.5	Phreato	fountain	120.	-	3	70	stratified	16	280	5	-	6	3

Reference	Unit		Composition	Emplacement					Structure						
(Di Vito *et al.* 2009) (Sulpizio *et al.* 2010)	Santo C	0	magmatic / Phreatomagmatic	collapse	0	0.65	5			/20 2020	- 300 300		-	5	0
	Volto Santo B	4.0	magmatic / Phreatomagmatic	fountain collapse	100.0	0.11	56	64	stratified	/2 11	- 320 300	-	-	5	45
	Volto Santo A	4.0	magmatic / Phreatomagmatic	fountain collapse	180.0	2.33	14	83	stratified	/1 2	- 320 260	8	-	7	175
	Tavernanova Terme	8.0	magmatic / Phreatomagmatic	fountain collapse	150.0	0.45	83	55	stratified	9/10	- 280 260	-	-	40	46
	Romane	5.01	magmatic / Phreatomagmatic	fountain collapse	200.0	--	-	--	stratified	8/10 11	- 280 280	-	-	40	46
	Nola	2.02	magmatic / Phreatomagmatic	fountain collapse	5.0	--	-	--	stratified	/1 9 11	- 300 280	-	-	37	54
	Afragola 13	0.02	magmatic / Phreatomagmatic	fountain collapse	30	--	-	--	stratified	/1 3	- 300 280	-	-	53	46
	Afragola 14	0.02	magmatic / Phreatomagmatic	fountain collapse	30	--	-	--	stratified	9/11 15	- 300 280	9	-	35	55
	Afragola H1	0.02	magmatic / Phreatomagmatic	fountain collapse	15	--	-	--	stratified	/1 5 10	- 300 260	-	-	64	00
	Afragola H3	0.02	magmatic / Phreatomagmatic	fountain collapse	15	--	-	--	stratified	/1 0 17	- 280 280	-	-	64	00
	Afragola H12	0.02	magmatic / Phreatomagmatic	fountain collapse	15	--	-	--	stratified	/2 0 13	- 320 280	-	-	45	551
	Afragola H17	0.02	magmatic / Phreatomagmatic	fountain collapse	15	--	-	--	stratified	/2 0 14	- 300 260	-	-	--	00
	Afragola H26	0.02	magmatic / Phreatomagmatic	fountain collapse	15	--	-	--	stratified	/1 6 12	- 280 360	-	-	36	82
Mercato (this paper)	PDC 8	MC9-2	4.8	Magmatic	total collapse	600	0.23	-	68	massive	/1 2 10	- 380 400	-	-	55	00
	PDc 7b	MC10-4	4.6	Magmatic	total collapse	55	1.43	-	50	massive	/1 1	- 420 380	-	-	37	00
	PDC 6	MC12	3.5	Magmatic	total collapse	150	0.60	-	55	massive	9/10 11	- 420 400	-	-	45	46
	PDC 5	MC10-1	4.6	Magmatic	total collapse	40	0.16	-	55	massive	/1 1 11	- 420 380	-	-	45	28
	PDC 4	MC9-2a	4.8	Magmatic	total collapse	40	0.04	-	60	massive	/1 1 11	- 400 360	-	-	36	64
	PDC 3	MC9-1	4.8	Magmatic	total collapse	60	0.51	-	70	massive	/1 2 13	- 400 360	-	-	81	28
Greenish (this paper)	F	VR4	3.6	Magmatic	total collapse	50	--	-	--	massive	/1 3	- 380	-	-	54	46

			MdΦ			F1					n/N	T$_{dep}$	A	B	C	D
Pomici di Base	EU5	VR4 Vallone di	3.6	Magmatic	total collapse	100.0	--	-	--	massive	27/29	340 360	-	-	52	48
(this paper)	EU4	Vallone di Pollena	3.5	Magmatic	fountain collapse	500.0	--	-	--	massive	14/16	340 380	-	-	25	75

Table 1 – Main sedimentological parameters and deposit temperature of PDCs deposits. Columns: D = distance from the vent; MdΦ = mean diameter; F1 = weight percentage of fractions finer than 1 mm; n/N = number of specimens used in T$_{dep}$ evaluation / number of measured specimens; T$_{dep}$ = deposit temperature; Type % (A, B, C,D) = type of clasts according to Cioni *et al.* 2004.

Eruption	Lithic clasts					Reference	Fine-grained matrix				Reference
	N/n	D (°)	I (°)	*k*	α$_{95}$ (°)		D (°)	I (°)	*k*	α$_{95}$ (°)	
1631 AD	1/1	4.0	56.5	32	8.4	this paper	2.0	65.0			Cafarella *et al.* 1992
Pollena	5/23	9.6	53.2	15	9.3	Zanella *et al.* 2008	4.7	53.7	259.6	0.8	Tanguy *et al.* 2003
Pompeii	1/6	359.2	56.8	251	4.2	Kent *et al.* 1981	356.4	56.5	1020	2.9	Kent *et al.* 1981
	8/87	354.4	57.2	433	2.7	Cioni *et al.* 2004	353.6	59.9	258	2.5	Zanella *et al.* 2000
Pompeii excavation	/75	352.0	53.7	--	4.9	Zanella *et al.* 2007	354.3	58.0	--	1.7	Zanella *et al.* 2007
Avellino	8/57	0.3	48.5	34	6.8	Di Vito *et al.* 2009	--	--	--	--	

Table 2 - TRM directions in lithic fragments and fine-grained matrix from pyroclastic deposits of the main Somma-Vesuvius eruptions. Symbols: N/n = number of sites/lithic fragments; D, I = declination, inclination; *k*, α$_{95}$ = precision, semi-angle of 95% confidence of Fisher's (1953) statistics. The direction reported for 1631 AD is the historical measurement by A. Kircher (Cafarella *et al.* 1992) relocated to Somma-Vesuvius via pole (Noel & Batt 1990).

	Volcanic parameters			PDC transport and deposition			
Eruption	**Volcanic explosive index**	**Magma chemistry**	**Magma temperature**	**PDC Volume**	**Furthest outcrop distance**	**Maximum runout**	**Cumulative maximum thickness**
	(VEI)			(km3)	(km)	(km)	(m)
1631 AD	4	Phonolitic tephrite to tephritic	1100-1150	0.20	7.8	>8, <10	18
Pollena	4	Phonolitic to phonolitic tephrite	850-900 1000-1100	0.39	8.6	>9, < 11	20
Pompeii	5	Phonolitic to phonolitic tephrite	850-900 1000-1100	0.83	20.5	~20.5	35
Avellino	5	Phonolitic to phonolitic tephrite		1.04	25.0	~25	22
Mercato	5	Phonolite	850-900	0.23	8.3	>8, <10	18
Greenish	4	Trachyte	850-900	>0,02	6.2	> 6	12
Pomici di Base	5	Trachyte to latite	850-900 950-1000	>0,18	5.8	> 6	25

Table 3 – Summary of main PDC parameters for each eruption, including magma composition and eruptive temperatures.